AIAA JOURNAL
Vol. 32, No. 4, April 1994

Numerical Model for Circulation-Control Flows

Richard G. Holz* and Ahmed A. Hassan†
McDonnell Douglas Helicopter Company, Mesa, Arizona 85205
and
Helen L. Reed‡
Arizona State University, Tempe, Arizona 85287

Current computational models for circulation-control flows have been applied, in most cases, to elliptical airfoils having only one blowing slot. This work describes a two-dimensional Navier-Stokes solver that has been developed for modeling the flowfields of a circular airfoil with two jets. In its original form, the Baldwin-Lomax algebraic turbulence model is shown to be inadequate for describing compound boundary layers such as those produced by the wall jet. A new turbulence model is therefore proposed. To account for the nonequilibrium production of turbulence at the slot exits and for its suppression due to wall curvature, two corrections to the turbulence model were implemented. A slanted slot exit boundary was used to reduce grid skewness without degrading solution accuracy. The current model has been validated for high-Reynolds-number/low-Mach-number flow over a circular cylinder with two jets. The model is shown to be valid over a wide range of slot flow conditions including stall. Some insight into wall jet separation is also presented.

Nomenclature

A^+ = 26
a = speed of sound
CC = wall curvature correction with $C_c = 25$
C_c = curvature correction constant
C_{cp} = 1.6
C_d = two-dimensional drag coefficient
C_{d_e} = $C_d + C_\mu (U_{jet}/2U_\infty)$
C_l = two-dimensional lift coefficient
C_{wk} = 0.25
C_μ = $2[(h_1 + h_2)/D](\rho_{jet}/\rho_\infty)(U_{jet}/U_\infty)^2$
$C_{\mu_{set}}$ = $C_\mu(\rho_\infty/\rho_{jet})$
D = circular airfoil diameter
h = slot height
K = 0.0168
l = turbulent eddy length scale
M = Mach number
PC = production correction with $\mu_{t_{jet}} = 150$ and $s_{off} = \pi/4$
PR = pressure ratio (slot total to freestream static)
p = pressure
Re = Reynolds number
s = circular arc length
TR = temperature ratio (slot static to freestream static)
U = velocity magnitude
y = normal distance from airfoil surface
α = angle of attack
η = normal coordinate in computational plane
μ = dynamic viscosity
ξ = surface coordinate in computational plane
ρ = density
ω = vorticity

Subscripts

dif = difference between adjacent vorticity minima
edge = relating to edge of viscous layer (i.e., where $|\omega| \approx 0.1$)
jet = relating to jet property at slot exit
l = laminar
max = relating to maximum vorticity point
min = relating to minimum vorticity point
off = where production correction terminates
slot = relating to a slot exit
t = turbulent or total
1 = relating to slot 1 exit
2 = relating to slot 2 exit
∞ = freestream condition

Superscripts

(1) = first viscous layer (wall)
(2) = second viscous layer (shear)
(3) = third viscous layer (shear)
+ = law-of-the-wall variable

Received Jan. 28, 1992; revision received Aug. 5, 1993; accepted for publication Aug. 26, 1993.

*Member, Technical Staff, Building 530, MS B346.
†Engineering Specialist, Building 530, MS B346.
‡Associate Professor, Mechanical and Aerospace Engineering Department. Associate Fellow AIAA.

Introduction

SINCE the first flight of the Wright brothers' flyer in 1903, aerodynamicists have been searching for practical means of generating not only increased lift but also increased control of lift. A natural outgrowth of the jet-blown flap research of the 1950s was the use of circulation control (CC): the practice of controlling the location of boundary-layer separation, and thus the circulation, with a tangentially blown jet of air on an "airfoil" that lacks a sharp trailing edge. Circulation control is employed in both the fixed- and rotary-wing industries. For example, the wing on the U.S. Navy's A-6 Crusader, the rotor on NASA's X-Wing, and the tailboom on McDonnell Douglas' NOTAR™ system all use CC for generating and controlling aerodynamic forces.

During the development of these and other applications of CC, much attention was focused on modeling the CC airfoil to predict its aerodynamic performance and to aid in its development. It has been shown that the quintessential feature of all CC flowfields, the wall jet, can be modeled fairly accurately as a separate entity.[1,2] However, the presence of a freestream flow surrounding the wall jet complicates the physics to such an extent that higher-order analytical models are required to produce meaningful predictions. The most promising models are generally classified as either inviscid / viscous interaction (IVI) methods or Navier-Stokes (NS) solvers. Some excellent IVI methods have been developed to date.[3–5] They are efficient and accurate and have been used to model the high-speed flowfields of the ellipse-shaped CC rotor. Several NS solvers have also been developed for the same purpose.[6–9]

Two major deficiencies stand out in the arena of CC flowfield modeling. First, it has been stated repeatedly that better turbulence models are needed in all of the methods developed to date.[9–11] Sec-

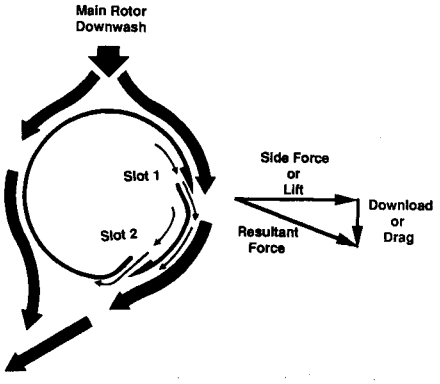

Fig. 1 Cross section of circulation control tailboom with two blowing shots.

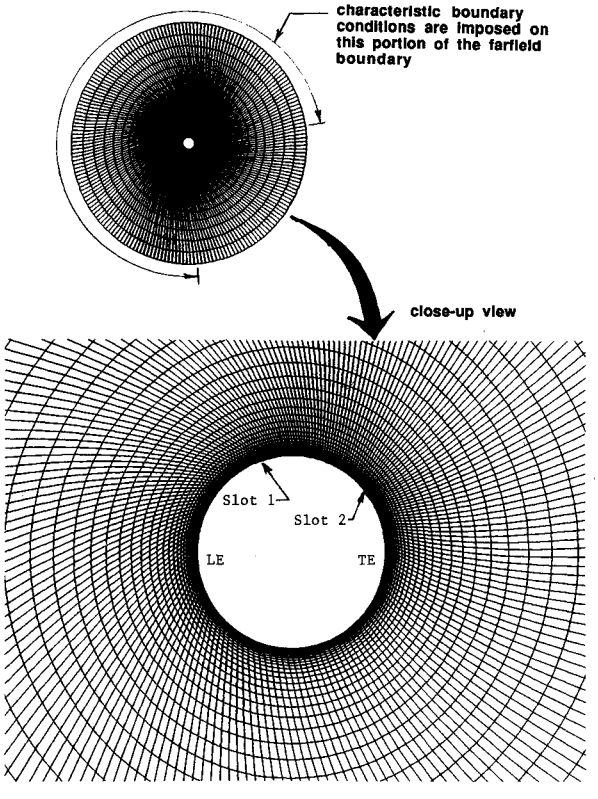

Fig. 2 Grid for circulation control airfoil with two blowing shots.

ond, it is clear that very little effort has gone into modeling the low-speed flowfield that occurs over the circular CC tailboom. Only two such efforts have been identified.[12,13]

The present paper addresses both of these deficiencies. A Navier-Stokes solver with a new turbulence model has been developed for a circular CC tailboom with two jets (see Fig. 1).The new turbulence model represents a considerable improvement over the industry-standard Baldwin-Lomax eddy viscosity model. Furthermore, the model has been used to optimize the aerodynamic performance of the CC tailboom and to study different types of wall jet separation.

Model Description

Mathematical Description

The governing equations are the two-dimensional Navier-Stokes equations for unsteady, viscous, and compressible flows. The equations are time averaged or Reynolds averaged to account for small-scale turbulence. This procedure leaves an unknown quantity, the eddy viscosity, to be determined by a turbulence model at every grid point location. The equations are nondimensionalized using the cylinder diameter as the length scale and the freestream speed of sound a_∞ as the velocity scale. The equations were retained in conservation form. To model the flow over any arbitrary body, we transformed the governing equations from the physical domain to a rectangular computational domain.

Numerical Formulation

The Beam and Warming[14] approximately factored, alternating-direction-implicit (ADI), time-marching procedure was used. The time and spatial derivatives were discretized using first-order forward differencing and second-order central differencing, respectively. The nonlinear flux terms were linearized using a first-order Taylor series expansion. The viscous terms were lagged by one time step; thus, the present formulation is not fully implicit. An artificial dissipation scheme similar to that proposed by Pulliam and Steger[15] was utilized. Here, second- and fourth-order dissipation terms were added to the right-hand side of the governing equations. These terms were evaluated explicitly. Moreover, second-order dissipation terms were added to the left-hand side of the resulting difference equations. A space-varying time step was also used to provide better-conditioned coefficient matrices and enhance numerical convergence.

The details of the mathematical and numerical formulations can be found in Ref. 16.

Computational Grid

All computations were performed on an O-type grid having 199 nodes on the surface of the airfoil (i.e., in the ξ-coordinate direction) and 61 nodes in the approximate normal direction to the surface (i.e., in the η-coordinate direction). Grid points were clustered on the surface of the airfoil, providing higher resolution in regions in the vicinity of the blowing slots. Exponential stretching along the surface was employed to insure smooth transition in grid point distribution. In the normal direction, the grid was stretched to resolve the viscous layer. More precisely, the normal grid spacing between the airfoil's surface and the first grid line off the surface

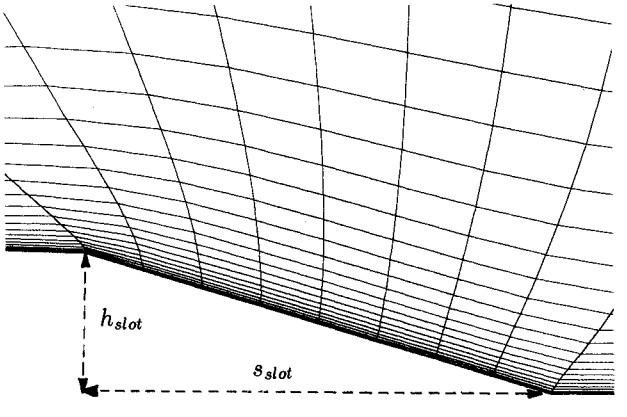

Fig. 3 Grid surrounding exit region of slot 2.

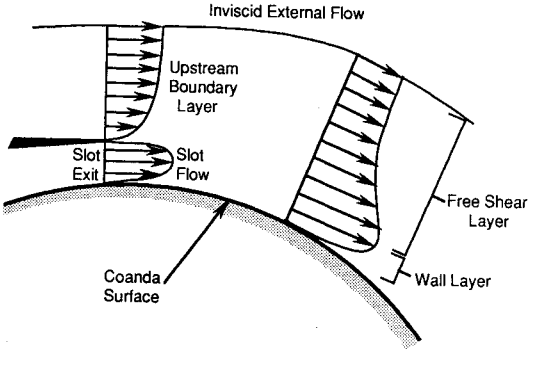

Fig. 4 Coanda surface terminology.

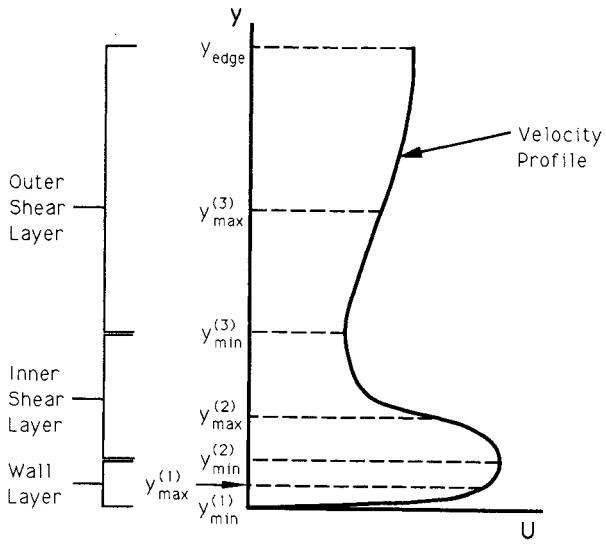

Fig. 5 Typical velocity profile in a type III wall-bounded layer.

was equal to 0.00007*D*. The outer far-field boundary was placed at a distance of 10 diameters away from the center of the airfoil. At the far-field boundary, the grid spacing in the normal direction was on the order of one diameter. Figure 2 illustrates the physical plane image of the computational grid generated for the circular airfoil with two slots.

In this study, the slots were modeled as a slanted boundary rather than by a perpendicular one. Figure 3 depicts the grid in the vicinity of the slanted slot exit. The ratio of slot length s_{slot} to slot height h_{slot} was no larger than 5 for any of the slots in the present study. Since wall jet separation would occur normally more than 100 slot heights downstream of the jet exit, the slanted geometry was not considered to be a detriment to the solution accuracy. On the contrary, by reducing the degree of grid skewness in the slot exit region, we obtained more accurate solutions.

Numerical Boundary Conditions

On the surface of the airfoil (excluding the slot exit), the no-slip boundary condition was enforced by setting the Cartesian velocity components to zero. The density and pressure on the solid surface were obtained by assuming that their normal gradients were zero at the wall. An adiabatic wall boundary condition was also used.

To avoid overspecification of the boundary conditions at the slot exit nodes, it was necessary to specify certain "internal" parameters (i.e., plenum conditions) and to allow for their interaction with the "external" flow environment to determine the boundary condition. The specified internal parameters were pressure ratio (slot total pressure to freestream static pressure), designated *PR*, and the temperature ratio (slot static to freestream static), designated as *TR*. These parameters were also convenient for the purpose of validating our model because they were measured in the experiment of Thompson.[17]

For the slot exit boundary condition, the static pressure was linearly extrapolated to each slot exit node from the adjacent field grid nodes. The local jet Mach number was then computed by inserting the ratio of the slot total to slot static pressure into the isentropic equation for pressure.The slot static temperature was then used to find the local speed of sound, which was then used in conjunction with the local Mach number to determine the magnitude of the local velocity. The Cartesian components of the jet velocity were obtained by stipulating that the slot flow exits in a direction tangent to the airfoil surface. Finally, the density was computed from the equation of state for an ideal gas.

A nonreflecting boundary condition[15] based on the characteristics of the two-dimensional inviscid Euler equations was used on 63% of the outer circular far-field boundary (see Fig. 2). A potential flow circulation correction, also suggested by Pulliam and Steger,[15] was applied to the freestream values of velocity and speed of sound to minimize the effect of the distance between the outer boundary and the airfoil on the solution accuracy. This is especially important for very high-lifting airfoils such as those employing circulation control.

For the subsonic, viscous flow found on the downstream boundary, the previous treatment is not valid. The generation of a viscous wake precludes the use of a boundary condition that is based on inviscid, characteristic theory. Instead, the density and the velocity components were set equal to those values at the neighboring interior nodes, and the pressure was fixed at its freestream value.

Turbulence Model

Figure 4 introduces some of the terminology that is essential to the following discussion. The Coanda surface is that portion of the CC airfoil to which the wall jet is attached.

The turbulence model developed for the present work is based on the assumption that three different types of wall-bounded layers may form on the Coanda surface of the CC airfoils considered here. All three have been observed experimentally.[18] Type I is a typical turbulent boundary layer, type II is a wall jet with two vorticity maxima (see Fig. 4), and type III is a wall jet with three vorticity maxima (see Fig. 5). Although the Baldwin-Lomax turbulence model[19] is well suited for type I profiles, it is not suitable for type II or type III profiles. This will be demonstrated by the authors' computations using the original and modified versions of the Baldwin-Lomax model.

Two shortcomings of the Baldwin-Lomax model are apparent. First, the *F*-function, given by

$$F(y) = y|\omega|[1 - \exp(-y^+/A^+)] \tag{1}$$

assumes the surface to be a reference point for determining length scales. This, however, is an invalid assumption for the free shear

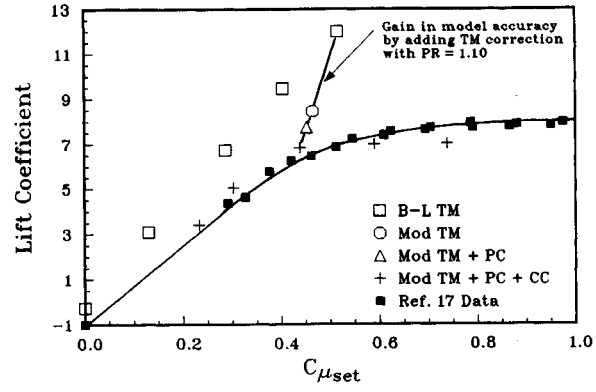

Fig. 6 $C_l - C_{\mu_{set}}$ computational results and experimental data.

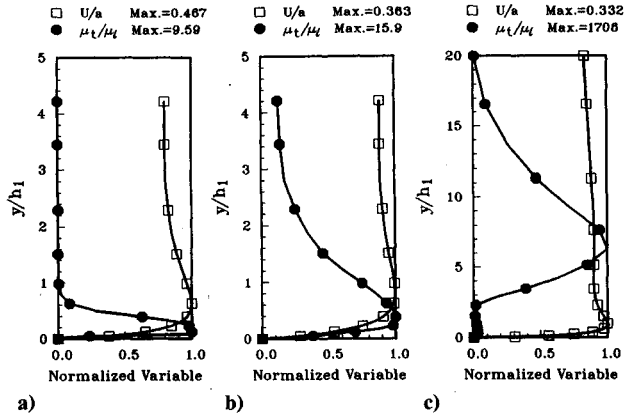

Fig. 7 Velocity and eddy viscosity profiles resulting from three different turbulence models: a) B-LTM, b) Mod TM, and c) Mod TM + PC + CC.

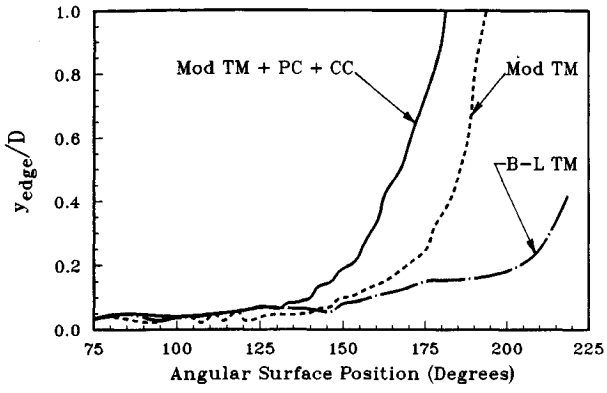

Fig. 8 Comparison of computed wall jet parameters resulting from two different turbulence models.

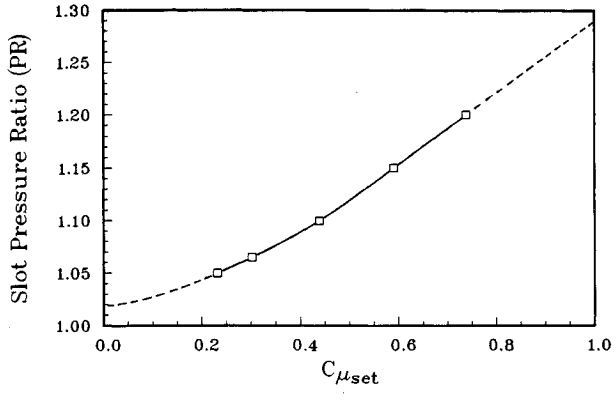

Fig. 9 Slot pressure ratio *PR* relationship to $C_{\mu_{set}}$ for circular cylinder with two slots placed 70 deg apart and $h_t/D = 0.0128$, $M_\infty = 0.1$, and $Re = 7 \times 10^5$.

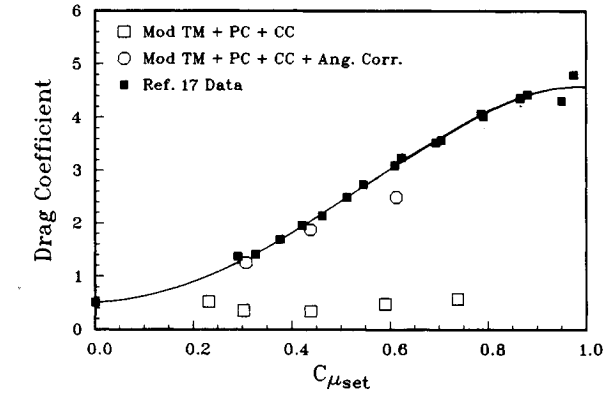

Fig. 10 $C_d - C_{\mu_{set}}$ computed results, with and without angularity correction, compared with experimental data.

layer portion of the wall jet. For this region, the length scale should be based, more appropriately, on the actual width of the shear layer. The second shortcoming of the Baldwin-Lomax model is that it uses the single largest peak in the F function to determine the peak level of viscosity. This approach can obviously lead to inaccuracies when double and triple peaks in the F function occur. Baldwin and Lomax alluded to this problem in their classic paper.[19]

Because of these shortcomings and the suggestions made by Dvorak,[18] a hybrid turbulence model was devised. In this model, the velocity profile type along each ξ = const coordinate line is determined from the number of vorticity maxima, and peak eddy viscosity levels corresponding to each local vorticity maximum are computed. The areas between vorticity maxima, use "transition" functions to assign eddy viscosities. The Klebanoff intermittency function was used for the transition between the fully turbulent and the nonturbulent regions of the flowfield.

The peak eddy viscosity associated with the wall layer is unchanged from the Baldwin-Lomax model, i.e.,

$$\mu_{t_{\max}}^{(1)} = \rho K C_{cp} y_{\max}^{(1)} F_{\max} \tag{2}$$

where $F_{\max}$ is the value of the wall layer F function peak and $y_{\max}^{(1)}$ is the value of y at which $F_{\max}$ occurs. Thus, the length and velocity scales are the same as those used in the original Baldwin-Lomax model for boundary layers.

The peak eddy viscosities for the outer shear layers are similar to those used in the wake formulation of the Baldwin-Lomax model, i.e.,

$$\mu_{t_{\max}}^{(2)\text{ or }(3)} = \rho K C_{cp} F_{\text{wake}} \tag{3}$$

where

$$F_{\text{wake}} = \min\left(l^2|\omega|_{\max},\ C_{wk}U_{\text{dif}}^2/|\omega|_{\max}\right) \tag{4}$$

The eddy length scale l is taken to be the normal distance from the local vorticity minimum to the local vorticity maximum for each zone. The parameter U_{dif} is the maximum difference in velocity across the shear layer. For example, in a type II profile U_{dif} is equal to $U(y_{\text{edge}}) - U(y_{\min}^{(2)})$. In a type III profile there are two free shear layers so that is U_{dif} is equal to $U(y_{\min}^{(3)}) - U(y_{\min}^{(2)})$V for one and $U(y_{\text{edge}}) - U(y_{\min}^{(3)})$ for the other.

The present turbulence model utilizes a correction term for the nonequilibrium production of turbulence at the slot exit and its convective transport downstream. Viegas et al.[9] used a similar term in their model. The nonequilibrium turbulence production is contained in an additional user-specified eddy viscosity term designated as $\mu_{t_{\text{jet}}}$. This eddy viscosity augments the peak eddy viscosity $\mu_{t_{\max}}$ given by Eqs. (2) and (3). Thus,

$$\mu_{t_{\max}}^{*} = \mu_{t_{\max}} + \mu_{t_{\text{jet}}} W f_r \tag{5}$$

where $\mu_{t_{\max}}^{*}$ is the corrected peak eddy viscosity for each wall jet layer, and f_r is a constant that controls the layer-by-layer distribution of this correction. The variable W is a damping function given by

$$W = 1 - (s/s_{\text{off}})^3 \tag{6}$$

where s_{off} is the user-specified arc length from the slot exit to the location where the correction terminates. If a separation point or the downstream jet is encountered before the s_{off} location, then the correction terminates at that point. The purpose of the factor W is to simulate the diminishing effect of the slot exit region as the fluid convects further downstream. This correction is applied over the entire viscous layer (i.e., from $y = 0$ to y_{edge}).

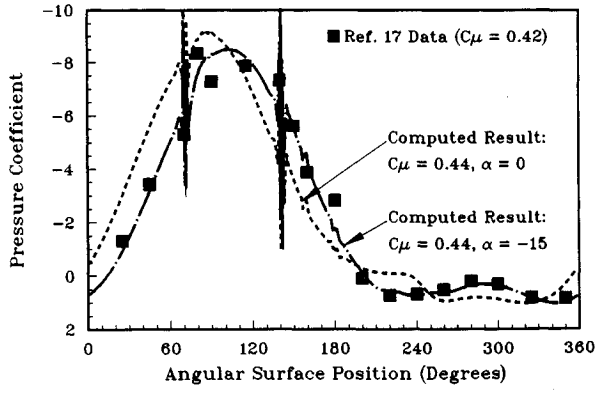

Fig. 11 Surface pressure comparison before and after angularity correction.

The effect of curvature on the turbulent shear stress has been well documented for both turbulent boundary layers[20] and wall jets.[21] To account for the curvature effect, we implemented a correction similar to that proposed by Pulliam et al.[7] as follows:

$$\mu_t = \sqrt{(\mu_t^*) - C_c \frac{U\omega l^4 \rho^2}{R_c}} \tag{7}$$

where μ_t^* is the corrected (i.e., for nonequilibrium production and convection) local eddy viscosity, C_c is a user-specified constant, and R_c is the local streamline radius of curvature. If the term under the radical in Eq. (7) became negative, then μ_t was automatically set to zero. Consequently, countergradient transport was not allowed in this model.

The present model is not valid in the vicinity of separation points or above the slot exits. Therefore, the eddy viscosities in these regions were computed using a linear interpolation scheme involving the eddy viscosities immediately adjacent to these areas. Additionally, the turbulence model occasionally produced unsmooth variations in the eddy viscosity with respect to both the η and ξ coordinate lines. To avoid this, we introduced a smoothing function to insure a smooth eddy viscosity distribution over the entire computational domain.

Results and Discussion

Turbulence Model Comparison

In our first attempts to compute CC flowfield solutions, the Baldwin-Lomax algebraic eddy viscosity turbulence model[19] (B-LTM) was used in its original form. The airfoil configuration that was used had two slots located at 70 and 140 deg (with respect to the freestream direction) with height to airfoil diameter ratios of 0.0036 and 0.0092, respectively. The freestream Mach number M_∞ and Reynolds number Re_∞ were 0.1 and 7×10^3, respectively. A temperature ratio of 1.054 was used. Pressure ratios of 1.00, 1.025, 1.05, 1.075, and 1.10 were imposed at the slot exit boundary.

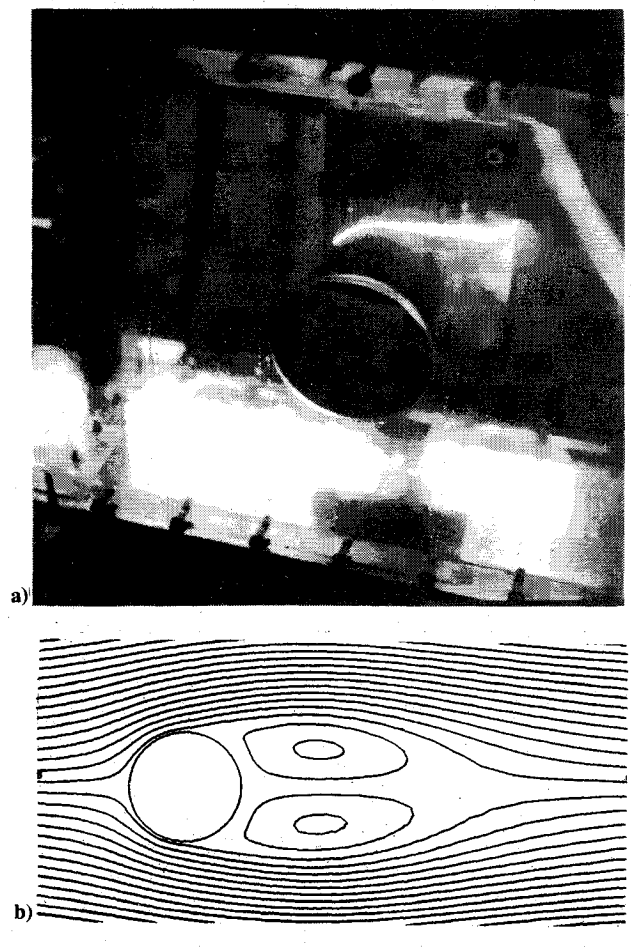

Fig. 12 High Reynolds number flow over a circular cylinder with no blowing: a) experimental flow visualization and b) computed streamlines.

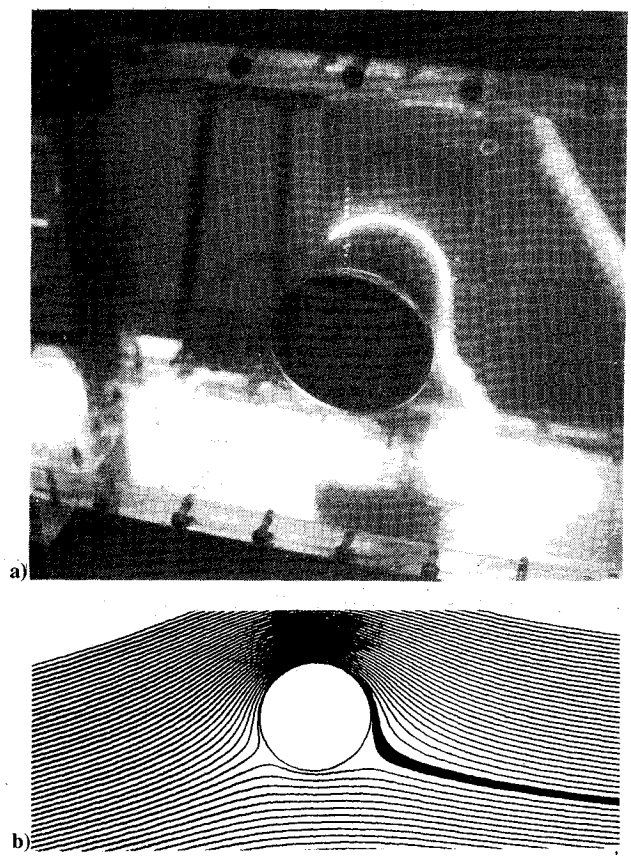

Fig. 13 High Reynolds number flow over a circular cylinder with blowing from two slots: a) experimental flow visualization and b) computed streamlines.

The resulting C_l vs $C_{\mu_{set}}$ (jet momentum coefficient) curve is plotted with the experimental data of Ref. 17 in Fig. 6. These results indicate that the computations that used the original Baldwin-Lomax model overpredict lift by as much as 70% and peak suction pressure by 80% at the larger values of $C_{\mu_{set}}$. Viegas et al.[9] reported a similar result when they used the B-LTM. Furthermore, the lift curve slope representing the computations provides no evidence of stall, whereas the experimental data indicate that the onset of stall occurs as the momentum coefficient approaches 0.4.

Figure 7a illustrates the wall jet profile that resulted from the original B-LTM for a station located at 20 slot heights downstream of the first slot. The quantities shown—total velocity and eddy viscosity to laminar viscosity ratio—have been normalized by the maximum value that occurs in the wall jet. The maximum values have been noted on the figure. Since high vorticity drives turbulence production, it is obvious that there is a lack of eddy viscosity assigned to the shear layer portion of the wall jet. This deficiency in the B-LTM led to the development of our turbulence model.

We began the development of our turbulence model by computing the $PR = 1.10$ case using the modified version with no corrections for the wall curvature or the nonequilibrium production of turbulence at the slot exit. The process proceeded by adding these corrections to our model one at a time. First, the constant, $\mu_{t_{jet}}$ (i.e., the production/convection correction), was incrementally increased from 0 to 300. For all of these calculations, s_{off} was set equal to $\pi / 4$. Afterward, it was discovered that for values of $\mu_{t_{jet}}$ greater than 150 no significant changes in C_l were produced. Therefore, with $\mu_{t_{jet}} = 150$, the curvature correction parameter C_c was varied from 0 to 100. A value of 25 for C_c produced the best correlations to the experimental data (i.e., it brought the predicted C_l to within 6% of the experimentally measured values).

The progression of our model's correlation with the experimental data of Ref. 17 is also illustrated in Fig. 6. Many of the steps in

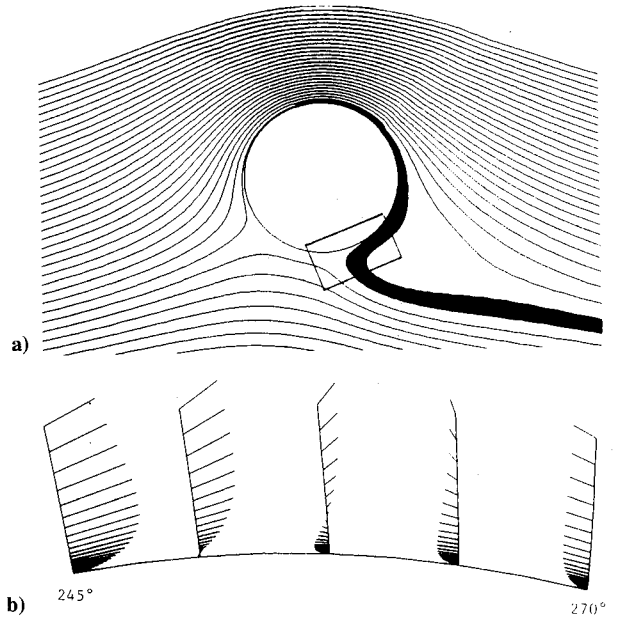

Fig. 14 $M_\infty = 0.1$ and $PR = 1.10$ case: a) stream function contours and b) velocity vectors.

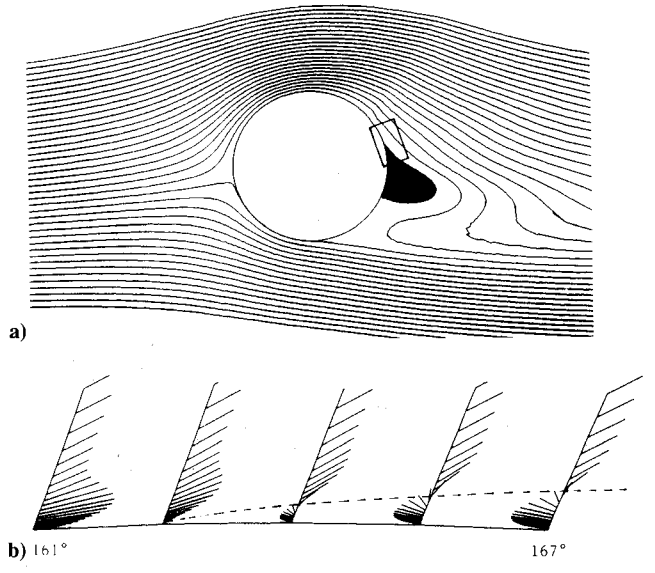

Fig. 15 $M_\infty = 0.3$ and $PR = 1.25$ case: a) stream function contours and b) velocity vectors.

our development process were omitted from this figure; only the steps that produced major improvements in the model's prediction capability were included. These improvements were caused by the elevated eddy viscosity levels in the shear layer. This is illustrated in Fig. 7. Figure 7a shows that the B-LTM assigns zero for the eddy viscosity in the shear layer. Figure 7b shows that our modified turbulence model assigns a nonzero eddy viscosity distribution in the shear layer. However, these eddy viscosities are still less than those in the wall layer. Figure 7c shows that, through the addition of the corrections for curvature and production/convection, the eddy viscosities in the shear layer are much larger than those in the wall layer. Figure 7 also illustrates the retardant effect that the increased eddy viscosity levels had on the wall jet. Although the shapes of the profiles are similar, the peak velocity in the wall jet diminished from 0.467 when the B-LTM was used to 0.332 when the modified turbulence model with corrections was used (recall that all velocities are nondimensionalized by the freestream speed of sound).

Figure 8 illustrates the increased thickening of the viscous layer caused by the modified turbulence model and the corrections. The parameter y_{edge} is defined as the point, while moving away from

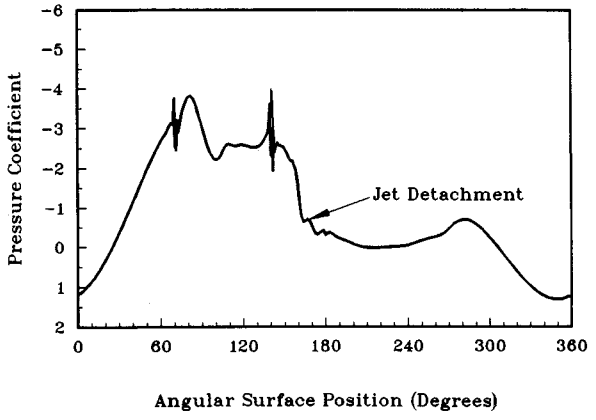

Fig. 16 Surface pressure distribution for $M_\infty = 0.3$ and $PR = 1.25$ case.

the airfoil surface, at which the nondimensional vorticity magnitude becomes less than 0.1. This is a good measure of where the viscous and inviscid layers merge. The displacement effect of the viscous layer is directly responsible for the decrease in circulation around the airfoil. This, in turn, results in the decreased suction pressures on the airfoil surface. Overall, the peak suction pressure decreased by about 40%. Consequently, the lift coefficient decreased by about the same percentage (recall Fig. 6).

Further manipulation of the turbulence model constants would have produced even better agreement with the experimental data. However, the parameters $\mu_{t_{jet}}$, s_{off}, and C_c were held constant at 150, $\pi/4$, and 25, respectively, to test the turbulence model's validity for a variety of freestream and slot flow conditions.

Note on Solution Convergence

All of the solutions computed for the present study utilized the space-varying "time" step. This was done to accelerate the solution convergence. The criteria that were used to determine if a steady state had been reached can be summarized as follows: 1) the maximum residual (change in conserved quantities in two consecutive iterations) was less than 10^{-5}, and 2) the lift and drag coefficients from two consecutive iterations changed by no more than 10^{-4}.

In most cases, it required more than 6000 iterations to obtain a steady-state solution. These slow convergence rates are not unprecedented for these types of flows. Viegas et al.[9] also reported slow convergence rates. They hypothesized the existence of a problem with solving a predominantly incompressible flowfield with a compressible solver. The present model is not an exception since it suffers from the same problem. For low-to-moderate blowing conditions (i.e., $PR \leq 1.10$), the integrated lift and drag coefficients would normally change only a few percent over several hundred iterations.

Validation Case: Two-Jet Circular Cylinder

The validation case for the circulation-controlled airfoil used the same airfoil configuration and freestream flow properties as those for the turbulence model comparison cases. The temperature ratio (i.e., 1.054) was representative of the experimental[17] ratios that ranged from 1.015 to 1.060. Five jet pressure ratios were considered: 1.05, 1.065, 1.10, 1.15, and 1.20. Figure 9 illustrates the relationship between momentum coefficient and pressure ratio that resulted from these particular cases. Converged solutions were obtained for all five cases.

The lift and drag results for the five computed cases, as well as the experimental data, are shown in Figs. 6 and 10, respectively. These figures illustrate that, although the lift coefficient is predicted remarkably well, the drag coefficients are far from the experimentally measured values. The noteworthy aspect of the lift curve is that it predicts the airfoil stall behavior with reasonable accuracy. Recall that the results generated with the original B-LTM in Fig. 6 indicated that no such phenomenon was present.

A representative surface pressure comparison at $C_{\mu_{set}} = 0.44$ is given in Fig. 11 (the various computed and experimental $C_{\mu_{set}}$ do not match exactly because the relationship between $C_{\mu_{set}}$, the result, and *PR*, the input, is not known a priori). For each of the cases considered, the computed pressure distributions matched the shape of the experimental distribution, but the positions of the stagnation points were shifted by 10–20 deg. Furthermore, the wind-tunnel data did not include any wall corrections, and significant three-dimensional effects were observed.[17] Therefore, it seemed reasonable to assume that a flow angularity existed that was not applied to the experimental lift and drag data. To test this theory, three additional cases were run at pressure ratios of 1.065, 1.10, and 1.15. For each case, a negative angle of attack equal to the estimated deviation in the position of the stagnation point was included. The motivation was to simulate the flow angularity in the wind tunnel and then to resolve the forces in "wind-tunnel coordinates."

The computed pressure distribution for $C_{\mu_{set}} = 0.44$ that included the flow angularity correction is also given in Fig. 11. These results support the hypothesis that there was considerable flow angularity in the wind tunnel. Although the lift coefficients were not affected significantly, the drag coefficients came in close agreement with the experimental data. The revised drag results, as resolved in wind tunnel coordinates, are compared with the experimental data in Fig. 10. This result indicates that wall effects should certainly be taken into consideration for CC wind-tunnel testing.

The streamline patterns shown in Figs. 12 and 13 qualitatively verify the validity of this model. In these figures, the computed streamline plots are compared with the flow visualization photographs from a recent water tank test. The freestream Reynolds numbers were about 7×10^5. Figure 12 shows the results for the case when no jet blowing was applied. The computed flowfield was unperturbed, thereby producing the steady, counter-rotating vortices shown in Fig. 12b. In Fig. 13, jet blowing was applied. In both cases, it is obvious that the computational model has produced nearly-accurate boundary layer and wall jet separation locations. The sizes of the wakes produced by the blown and unblown cylinders also appear to be modeled accurately.

Two Types of Wall Jet Separation

One of the outstanding features of this numerical model is its ability to simulate flowfields produced by very different boundary conditions. For example, when a low freestream Mach number (i.e., 0.1) is coupled with a moderate momentum coefficient (i.e., 0.44), the type of flowfield depicted in Fig. 14 results. Here, the wall jet separates from the airfoil because it is "overpowered" by the lower surface boundary layer. The velocity vectors in Fig. 14 indicate that the wall jet and lower surface boundary layer merged without forming a separation bubble on the lower surface of the airfoil. "Angle of attack stall" occurs when the airfoil is rotated in a sense that brings the trailing slot closer to the lower surface boundary layer, thus preventing the airfoil from producing additional lift.

When a high freestream Mach number (i.e., 0.3) and a relatively low momentum coefficient (i.e., 0.1) are present, the type of flowfield depicted in Fig. 15 results. Here, the wall jet abruptly detaches from the airfoil surface and forms a separation bubble. The detachment point is approximately located at 163 deg, only 23 deg downstream of the second slot. The surface pressure distribution in Fig. 16 illustrates how this type of detachment creates a significant loss of suction between the slots. Wood and Nielsen[11] have pointed out that the increased Mach number creates an accentuated upstream pressure gradient that, in turn, causes thickening of the upstream boundary layer. The combination of the ill-conditioned boundary layer and the weak jet results in the failure of the Coanda effect.

Closing Remarks

Some progress has been made in the modeling and understanding of circular CC airfoils with two jets. The universality of the present model has not been fully tested; however, it is worth noting that the same turbulence model constants were used to produce all of the results presented herein. Although there is still a need for turbulence model improvement, the one presented here predicted much of the CC airfoil behavior that was observed in experiments. We have demonstrated that relatively simple algebraic turbulence models can simulate wall jet physics well enough to produce fairly accurate predictions of CC airfoil performance.

Acknowledgments

The first author was supported on this research by the McDonnell Douglas Helicopter Company/Arizona State University Industrial Fellows Program. The authors would like to thank L. N. Sankar of the Georgia Institute of Technology for his suggestions.

References

[1]Glauert, M. B., "The Wall Jet," *Journal of Fluid Mechanics,* Vol. 1, May 1956, pp. 625–643.

[2]Roberts, L., "A Theory for Turbulent Curved Wall Jets," *Proceedings of the Circulation-Control Workshop* (Moffett Field, CA), NASA CP 2432, Feb. 1986, pp. 99–112.

[3]Dvorak, F. A., and Kind, R. J., "Analysis Method for Viscous Flow over Circulation-Controlled Airfoils," *Journal of Aircraft,* Vol. 16, No. 1, 1979, pp. 23–28.

[4]Dvorak, F. A., and Choi, D. H., "Analysis of Circulation-Controlled Airfoils in Transonic Flow," *Journal of Aircraft,* Vol. 20, No. 4, 1983, pp. 331–337.

[5]Dvorak, F. A., and Dash, S. M., "Wall Jet Analysis for Circulation Control Aerodynamics—Part II: Zonal Modeling Concepts for Wall Jet/Potential Flow Coupling," *Proceedings of the Circulation-Control Workshop* (Moffett Field, CA), NASA CP 2432, Feb. 1986, pp. 165–181.

[6]Berman H. A., "A Navier-Stokes Investigation of a Circulation Control Airfoil," AIAA Paper 85-0300, Jan. 1985.

[7]Pulliam, T. H., Jespersen, D. C., and Barth, T. J., "Navier-Stokes Computations for Circulation Control Airfoils," *Proceedings of the Circulation-Control Workshop* (Moffett Field, CA), NASA CP 2432, Feb. 1986, pp. 135–153.

[8]Shrewsbury, G. D., "Evaluation of a Research Circulation Control Airfoil Using Navier-Stokes Methods," AIAA Paper 87-0002, Jan. 1987.

[9]Viegas, J. R., Rubesin, M. W., and MacCormack, R. W, "On the Validation of a Code and a Turbulence Model Appropriate to Circulation Control Airfoils," AGARD Symposium on Validation of Computational Fluid Dynamics, Paper 6, Lisbon, Portugal, May 2–5, 1988.

[10]Nielsen, J. N., and Biggers, J. C., "Recent Progress in Circulation Control Aerodynamics," AIAA Paper 87-0001, Jan. 1987.

[11]Wood, N., and Nielsen, J., "Circulation Control Airfoils—Past, Present, and Future," AIAA Paper 85-0204, Jan. 1985.

[12]Morger, K. M., and Clark, D. R., "Analytic and Experimental Verification of the NOTAR™ Circulation Control Tail Boom," presented at the 40th Annual Forum of the American Helicopter Society (Washington, DC), May 1984.

[13]Tadghighi, H., and Thompson, T. L., "Circulation Control Tail Boom Aerodynamic Prediction and Validation," presented at the 45th Annual Forum of the American Helicopter Society (Boston, MA), May 1989.

[14]Beam, R. M., and Warming, R. F., "An Implicit Factored Scheme for the Compressible Navier-Stokes Equations," *AIAA Journal,* Vol. 16, No. 4, April 1976.

[15]Pulliam, T. H., and Steger, J. L., "Recent Improvements in Efficiency, Accuracy, and Convergence for Implicit Approximate Factorization Algorithms," AIAA Paper 85-0360, Jan. 1985.

[16]Wu, J. C., "A Study of Unsteady Turbulent Flow Past Airfoils," Ph.D. Dissertation, School of Aerospace Engineering, Georgia Inst. of Technology, Atlanta, GA, Aug. 1988.

[17]Thompson, T. L., "Wind Tunnel Study of a Circular Cylinder with Two Tangentially Blowing Slots," McDonnell Douglas Helicopter Co., Aeromechanics Technical Note 87-047, Mesa, AZ, July 1987.

[18]Dvorak, F. A., "Calculation of Turbulent Boundary Layers and Wall Jets over Curved Surfaces," *AIAA Journal,* Vol. 11, No. 4, 1973, pp. 517–524.

[19]Baldwin, B. S., and Lomax, H., "Thin Layer Approximation and Algebraic Model for Separated Turbulent Flows," AIAA Paper 78-257, Jan. 1978.

[20]Moroney, R. N., and Bradshaw, P., "Turbulent Boundary Layer Growth over a Longitudinally Curved Surface," *AIAA Journal,* Vol. 13, No. 11, 1975, pp. 1448–1453.

[21]Wilson, D. J., and Goldstein, R. J., "Turbulent Wall Jets with Cylindrical Streamwise Surface Curvature," *Journal of Fluids Engineering,* Vol. 98, Sept. 1976, pp. 550–557.